phys. stat. sol. (a) 82, 35 (1984)

Subject classification: 7; 14.4.1; 22.8.1

Hamburger Synchrotronstrahlungslabor HASYLAB at
Deutsches Elektronen-Synchrotron DESY, Hamburg[1])

Contrast Investigations of Surface Acoustic Waves by Stroboscopic Topography

I. Orientation Contrast

By
H. CERVA[2]) and W. GRAEFF

Surface acoustic waves are investigated by stroboscopic topography using synchrotron radiation from the storage ring DORIS. The observed contrast of the acoustic displacements of the lattice planes has the same periods as the acoustic wave. It is demonstrated that the major part of the contrast is due to orientation contrast of the curved net planes. Intensity maxima correspond to troughs of the acoustic wave, minima to crests. A numerical treatment yielding ray tracing maps, intensity curves as well as focusing conditions which are in quantitative agreement with the experimental data are presented.

Akustische Oberflächenwellen werden mittels stroboskopischer Röntgentopographie untersucht. Dazu wird die Synchrotronstrahlung des Speicherrings DORIS benutzt. Der beobachtete Kontrast, der durch die akustische Verschiebung der Netzebenen entsteht, hat die gleiche Periodizität wie die akustische Welle. Es wird gezeigt, daß der Hauptanteil des Kontrastes durch Orientierungskontrast der deformierten Netzebenen zustande kommt. Die Intensitätsmaxima entsprechen den Tälern der Oberflächenwelle, die Minima den Bergen. Eine numerische Behandlung ermöglicht die Berechnung der Strahlwege und damit die Simulation des Kontrastes. Außerdem erhält man einen Ausdruck für den Intensitätsverlauf und Fokussierungsbedingungen, die mit den experimentellen Ergebnissen quantitativ übereinstimmen.

1. Introduction

During the last two years X-ray topography experiments using a stroboscopic technique have been performed in the MHz region using the time structure of synchrotron radiation. Glüer et al. [1] studied standing bulk waves and their effect on the image formation of dislocations in quartz. Whatmore et al. [2, 3] made use of this new method when imaging travelling surface acoustic waves (SAW) on a $LiNbO_3$ television IF filter. At present the scanning electron microscope (SEM) working in the stroboscopic voltage contrast mode as introduced by Feuerbaum et al. [4, 5] is the most important tool to control SAW device performance.

Though travelling waves can be visualized in the SEM no information concerning crystallographic defects and strains in the substrate can be obtained. Stroboscopic X-ray topography, however, permits to image the surface waves, crystal defects, and mechanical deformations simultaneously.

From our investigations on a similar $LiNbO_3$ device we found that the characteristics of the wave contrast formation need explanation first. Then it is evident which conditions and effects should be noticed to make quantitative statements on surface wave propagation and its interaction with crystal properties.

[1]) Notkestr. 85, D-2000 Hamburg 52, FRG.
[2]) On leave from Inst. f. Angewandte u. Techn. Physik, Techn. Universität Wien, A-1040 Wien, Austria.

2. The Stroboscopic Technique

Synchrotron radiation from storage rings has a very pronounced time structure as the circulating particles (electrons or positrons) are concentrated in so-called bunches. Two parameters of this time structure are fixed and one can assume certain predefined values. The fixed parameters are circulation time of an individual bunch and its length, in case of DORIS 960 ns and 150 ps, respectively. The variable parameter is the number N of stored bunches which at DORIS can vary between 1 and 480 with the restriction that $480/N$ is an integer. Hence the pulse repetition time varies between 2 ns ($N = 480$) and 960 ns ($N = 1$).

Most of our experiments have been performed with the storage ring running in single-bunch mode which offers the greatest flexibility for stroboscopic topography as phenomena of n times the source frequency can be investigated.

The key to stroboscopic topography is the exact synchronization of the observed process, here surface acoustic waves, to the time structure of the source. The latter is defined by a master oscillator which controls the HF cavities of the storage ring (see Fig. 1). From this oscillator a bunch trigger signal is derived to phaselock a frequency synthesizer via its external clock input to 1.040968 MHz, the frequency of a reference bunch. The frequency synthesizer can produce multiples of this fundamental frequency up to 1 GHz. A subsequent broad-band amplifier delivers the driving signal for the sample up to 15 V amplitude. A variable delay allows for changing the phase relation between the bunch trigger and the actual photon pulse arrival in steps of 2 ns.

As the typical exposure time in our experiments was about 1 s, purely periodic processes can be imaged by this technique with time resolution of the order of nanoseconds but any irreversible phenomenon occurring on a time scale shorter than the exposure time will obviously not be visible.

3. Rayleigh Waves on Lithium Niobate

Surface acoustic waves are elastic waves propagating on the surface of a solid or liquid medium (e.g. Rayleigh waves) [6]. For SAW applications this medium is a piezoelectric, anisotropic crystal. By means of an interdigital transducer (IDT) — an array of conducting strips deposited on the crystal surface — electromagnetic signals generate surface waves due to the inverse piezoelectric effect (Fig. 2).

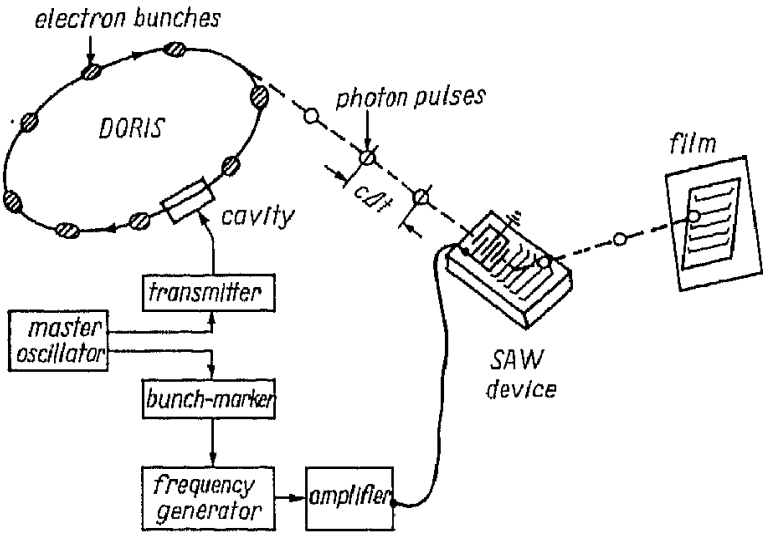

Fig. 1. Scheme of the stroboscopic technique. The SAW is synchronized to the incident photon pulses resulting in a standing wave pattern on the film

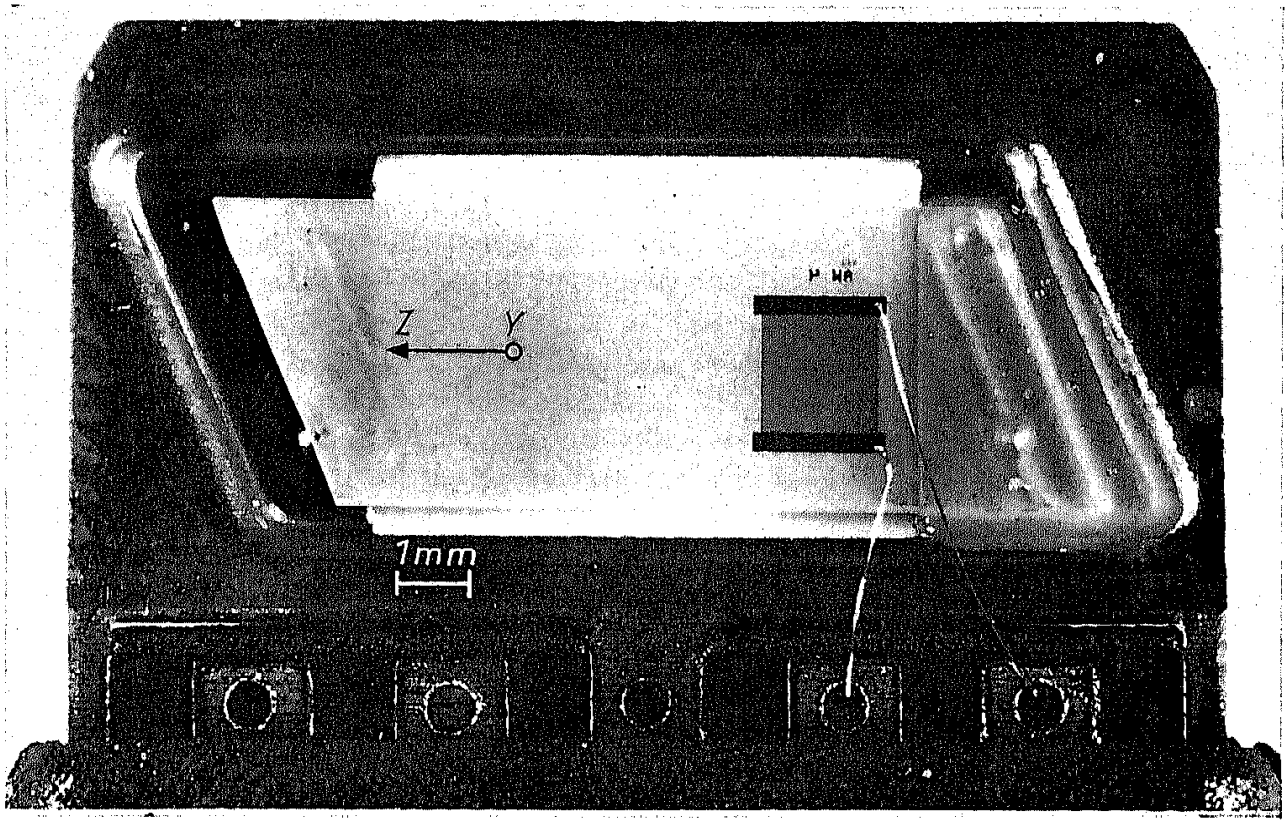

Fig. 2. Photomicrograph of the 35 MHz YZ $LiNbO_3$ SAW device with a single interdigital transpucer

The linear theory of elasticity permits to describe elastic waves in a charge-free piezoelectric solid. These waves are found by solving a system of four coupled wave equations for the three elastic displacements u_j and the electric potential φ. At large depth of the crystal u_j and φ should vanish. At the surface which is assumed not to be metallized the potential should be continuous and fulfil Laplace's equation outside the crystal. Usually the solution for SAW is written as a linear combination of partial waves,

$$\begin{aligned} u_j &= \{\sum C^{(n)}\alpha_j^{(n)} \exp(iKb^{(n)}x_3)\} \exp[iK(x_1 - vt)]; \qquad j = 1, 2, 3, \\ \varphi &= \{\sum C^{(n)}\alpha_4^{(n)} \exp(iKb^{(n)}x_3)\} \exp[iK(x_1 - vt)], \end{aligned} \tag{1}$$

where K is the acoustic wave number, v the phase velocity, $C^{(n)}$ weighing coefficients, $\alpha_j^{(n)}$ the amplitudes, and $b^{(n)}$ the decay constants of the partial waves. The geometry is explained in Fig. 3. A procedure how to find the solution is outlined in [6].

The motion of an individual atom in an arbitrary SAW is elliptical. At the surface the elliptical motion is retrograde and changes its sense of circulation deeper in the substrate.

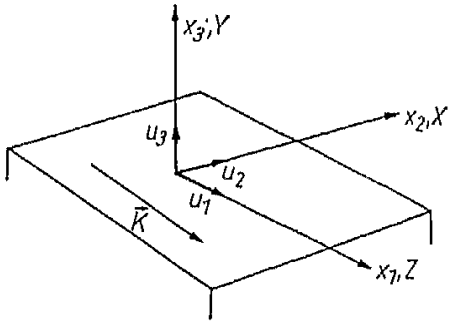

Fig. 3. X, Y, Z are rectangular crystal axis while x_1, x_2, x_3 are the coordinates of an orthogonal system defining SAW propagation in the Y cut, Z propagating case. $\boldsymbol{K}$ is the acoustic wave vector

For Y-cut, Z-propagation $LiNbO_3$ (trigonal 3m, space group R3c) the wave equations decouple and only the components u_1, u_3, and φ form the SAW. The component u_2 gives an additional transversely polarized bulk wave. The particle motion of the SAW lies in the sagittal plane (YZ plane) and u_1 and u_3 are nearly in phase quadrature. We have calculated the partial wave constants mentioned above for the case of YZ $LiNbO_3$. The values are given in Table 1 (values for $n = 4$ are omitted as they do not contribute to the SAW in this case). They are normalized to $u_3(0) = 1$. The absolute squared values of the surface displacement amplitudes for YZ $LiNbO_3$ are

$$\frac{|u_j(0)|^2\,\omega}{4P} = c_j; \qquad j = 1, 3\,, \tag{2}$$

given in [6], with $c_1 = 3.16 \times 10^{-12}\,\mathrm{m^3J^{-1}}$ and $c_3 = 6.86 \times 10^{-12}\,\mathrm{m^3J^{-1}}$. ω is the frequency of the SAW and P the power per unit width carried in the wave parallel to the propagation direction. In order to estimate $|u_j(0)|$, $j = 1, 3$ corresponding to a voltage U_{in} applied to the IDT we assume that $|u_j(0)|$ increases linearly with U_{in} (which might be false for large U_{in} due to anharmonic effects). The input power P_{in} is given by

$$P_{in} = \frac{U_{in}^2 G(\omega)}{2}\,, \tag{3}$$

where U_{in} is the peak applied voltage and $G(\omega)$ the frequency dependent input conductance.

This power is completely converted into acoustic power of the SAW if the number of finger pairs in the IDT is sufficiently large [7]. Then we may write

$$P = \frac{P_{in}}{2a}\,, \tag{4}$$

where a is the aperture of the IDT. This yields

$$|u_j(0)| = \frac{1}{2}\left(\frac{c_j G(\omega)}{\omega a}\right)^{1/2} U_{in}\,. \tag{5}$$

For the next sections we define the abbreviations $a_1 = |u_1(0)|$ and $a_t = |u_3(0)|$.

Table 1

Partial wave constants for a SAW on YZ $LiNbO_3$, $v = 3488$ m/s

n	$b(n)$	j	$C(n)\,\alpha_j(n)$
1	$0.3804 - i\,1.0378$	1	$-0.324 - i\,0.497$
		2	0.0
		3	$-0.078 + i\,0.360$
		4	$-0.781 + i\,0.211$
2	$-0.3959 - i\,0.7738$	1	$0.392 - i\,0.269$
		2	0.0
		3	$0.098 - i\,0.500$
		4	$0.734 + i\,0.480$
3	$0.0646 - i\,0.1218$	1	$-0.064 + i\,0.088$
		2	0.0
		3	$0.980 + i\,0.139$
		4	$0.089 - i\,0.139$

4. Experiments

For our experiments we used YZ $LiNbO_3$ devices as shown in Fig. 2 equipped with one IDT only. We had IDTs with different center frequencies (35 and 56 MHz) and substrates of different crystal quality at our disposal. The substrate was chosen such that no grain boundaries or ferroelectric domains impaired the wave excitation or propagation. In order to avoid strains and torsions the plate was glued onto the mounting at its right edge only. Both edges were then covered with an adhesive acting as an acoustic absorber. The complete device was fixed on a goniometer.

Experiments have been performed at the white beam topography station at HASYLAB. The electron energy of the storage ring DORIS was 5 GeV with an average current of 17 mA. Two types of photographic material were used, single coated Kodak Industrex R film and Ilford L. 4 nuclear emulsion plates. The exposure times were about 0.5 s for the Kodak film and two to three times longer for the nuclear plate. The distance from the sample to the source is 34 m and the source size is about 2 mm vertically and 4 mm horizontally. The film was placed 5 to 20 cm behind the sample which was set for taking reflection topographs in the vertical diffraction plane because of the intrinsic polarization of the synchrotron radiation beam. The crystal was exposed to the white beam. Therefore, one has to take into account the superposition of several harmonics in each Laue spot.

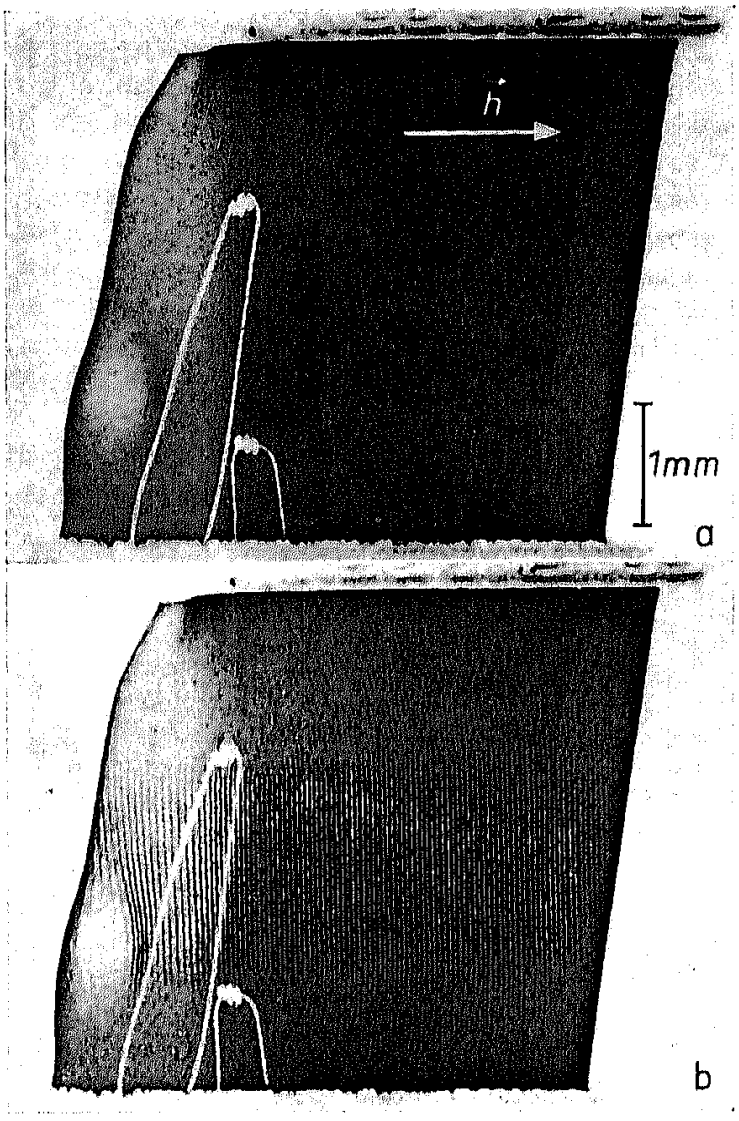

Fig. 4. (a) Reflection topograph of the device shown in Fig. 2 (Kodak R film) 24 mA, 0.2 s exposure time, $\theta = 25°$, (03.0) reflection. h indicates the projection of the diffraction vector onto the film; b) same as a), but with SAW excitation

We concentrated on the $(0k.0)$ reflections, $k = 3, 6, \ldots$, which represent net planes parallel to the YZ $LiNbO_3$ surface. This gives a symmetric Bragg case with the SAW amplitudes a_t normal to the surface and a_l parallel to the Z-axis.

Fig. 4 shows two reflection topographs from the same crystal. In topograph a no surface waves are excited. Each conducting wire gives rise to two shadows because they are illuminated by the incident and reflected beam simultaneously. The crystal has a dislocation density of about 10^4 cm^{-1} (or even higher — because of invisible dislocations) and no grain boundaries. The left side of the topograph appears much brighter and the edge is no straightline. This is the side where the crystal is fixed to the mounting. The distortions give a strong orientation contrast. The adhesive on the edges of the sample absorbs photon intensity as can be seen on the right side of the topograph. The IDT is visible as a more strongly reflecting area because of the strains induced by the electrode structure.

In topograph b surface waves are excited at 35.4 MHz with 15 V_{pp}. On the left part of the topograph where the waves pass the strongly distorted surface the orientation contrast can be observed best. Depending on the sense of the curvature of the net planes the spacing of the acoustic wave fronts appears broader or narrower. The oblique edge reflects surface waves despite of the adhesive. In addition the IDT excites spurious waves propagating along the X-axis. The fact that they are visible in the (03.0) reflection indicates a displacement component perpendicular to the surface.

The contrast formation of the SAW is demonstrated by the following experiment. A wire of 25 μm diameter was placed in front of the crystal at a height of about 1 mm inclined to the propagation direction of the SAW. The illumination condition was as illustrated in Fig. 5 a so that the wire casts two shadows s_1 and s_2 onto the film. When comparing with the topograph in Fig. 5 b s_1 has wavy but sharp borders. The troughs of the surface wave bring the reflected X-rays into focus, the crests defocalize, which explains the wavy shape. Shadow s_2, however, already occurs in the incident beam and its border lines give a diffuse image. This additional contrast arises from the penetrating wave fields which are deflected by the strain field of the SAW and emerge in area s_2'. This phenomenon has been investigated in case of homogeneous [8] and dislocation strain fields [9] and will be considered for this particular case in Part II of this paper.

5. Orientation Contrast Formation

Usually the extinction length Δ_e which measures the thickness of the surface layer of the crystal which builds up the reflected beam is small compared to the acoustic wave-

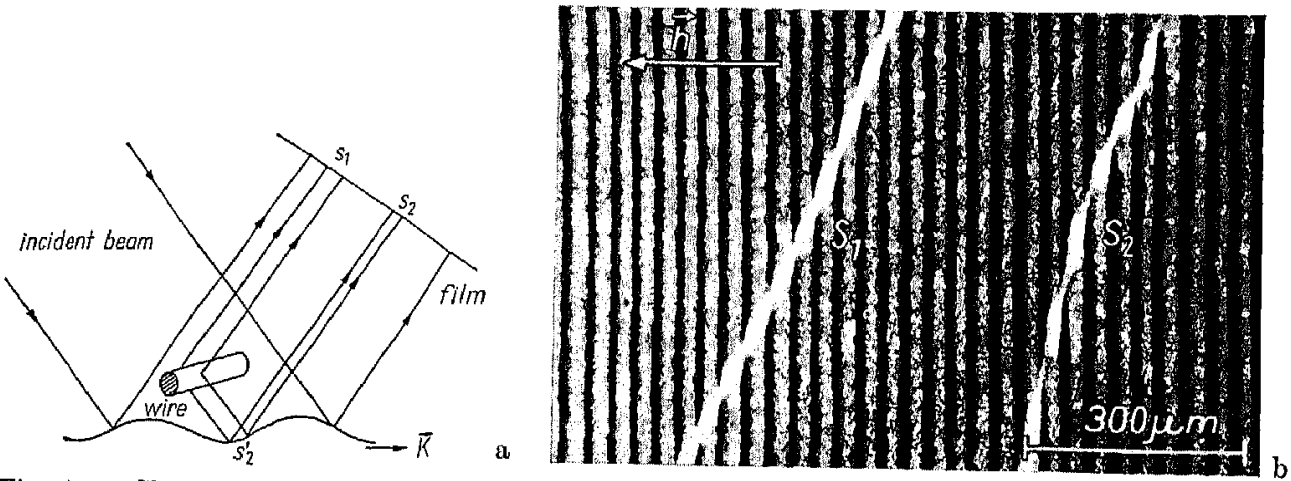

Fig. 5. a) Sketch how the two shadows in topograph b) are formed. b) Reflection topograph (Kodak R film) 18 mA, 0.3 s exposure time, $\theta = 35°$, (03.0) reflection. The wire diameter was 25 μm

length Λ. For instance, in the case of a 35 MHz IDT on YZ $LiNbO_3$ considered above we have approximately $\Lambda = 100\ \mu m$ and for the 03.0 reflection with $\lambda = 0.18$ nm the extinction length $\Delta_e = 6\ \mu m$. Even with the second order 06.0 ($\lambda = 0.09$ nm), $\Delta_e = 22\ \mu m$ is still a small fraction of the acoustic wavelength. In this case the curvature of the net planes due to a travelling Rayleigh wave does not change very much over the extinction length.

We then may approximate the Bragg reflection from a set of net planes parallel to the surface (symmetric Bragg case) by a simple mirror reflection from a corrugated surface. We neglect the changing lattice orientation inside the crystal which is seen by a penetrating wave field. This effect can be separated from the surface reflected beam as demonstrated in Fig. 5 and will be discussed in Part II of this paper. The orientation contrast can be investigated by ray tracing calculations.

For this purpose we define a coordinate system with the xy-plane forming the undisturbed crystal surface. The xz-plane defines the scattering plane although small y components are allowed. This coordinate system differs from the one used in the previous section by a rotation about the z-axis. Thus the acoustic wave propagation is not bound to the scattering plane. A source point is located at $R_s = (-L \cos\theta, 0, L \sin\theta)$, a distance L away from the crystal. The unit vector $\hat{\mathbf{s}}_0 = (\cos\theta, 0, -\sin\theta)$ points from the source to the origin. The angular deviation of a ray with respect to $\hat{\mathbf{s}}_0$ is expressed by angles ψ and φ, ψ lying in the xz-plane and φ perpendicularly. Hence the ray direction is $\mathbf{s}_0 = \hat{\mathbf{s}}_0 + \Delta\mathbf{s}_0$ with $\Delta\mathbf{s}_0 = (-\psi \sin\theta, \varphi, -\psi \cos\theta)$. This ray hits the crystal surface at $r_c = (-L\psi/\sin\theta, L\varphi, 0)$ (see Fig. 6).

The Rayleigh wave is expressed in coordinates $r_c = (x, y)$ of the unperturbed crystal surface,

$$r = (x - a_l \cos\beta \sin\Phi,\ y - a_l \sin\beta \sin\Phi,\ a_t \cos\Phi) \tag{6}$$

with

$$\Phi = r_c K = \left(LK\varphi \sin\beta - \psi \frac{\cos\beta}{\sin\theta}\right),$$

β is the angle of the acoustic wave vector $\boldsymbol{K}$ towards the x-axis.

The local surface normal $\boldsymbol{n}$ is parallel to the vector $\boldsymbol{f} = (\partial\boldsymbol{r}/\partial x) \times (\partial\boldsymbol{r}/\partial y)$ which is evaluated to

$$\boldsymbol{f} = (a_t K \cos\beta \sin\Phi,\ a_t K \sin\Phi,\ 1 + a_l K \cos\Phi) \tag{7}$$

and

$$f = |\boldsymbol{f}| = \sqrt{1 + 2a_l K \cos\Phi + K^2(a_l^2 \cos^2\Phi + a_t^2 \sin^2\Phi)}\,.$$

Neglecting terms of second order in the amplitude we obtain

$$\boldsymbol{n} = \frac{\boldsymbol{f}}{f} = (a_t K \cos\beta \sin\Phi,\ a_t K \sin\beta \sin\Phi,\ 1)\,. \tag{8}$$

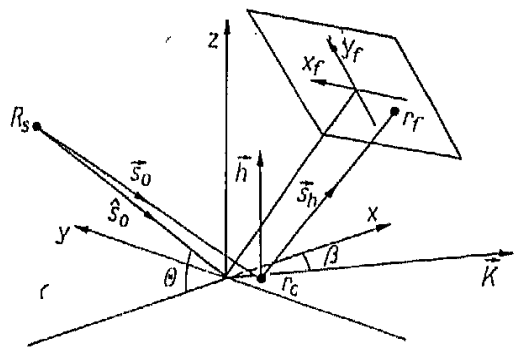

Fig. 6. Coordinate systems used to simulate orientation contrast. Letters are explained in the text

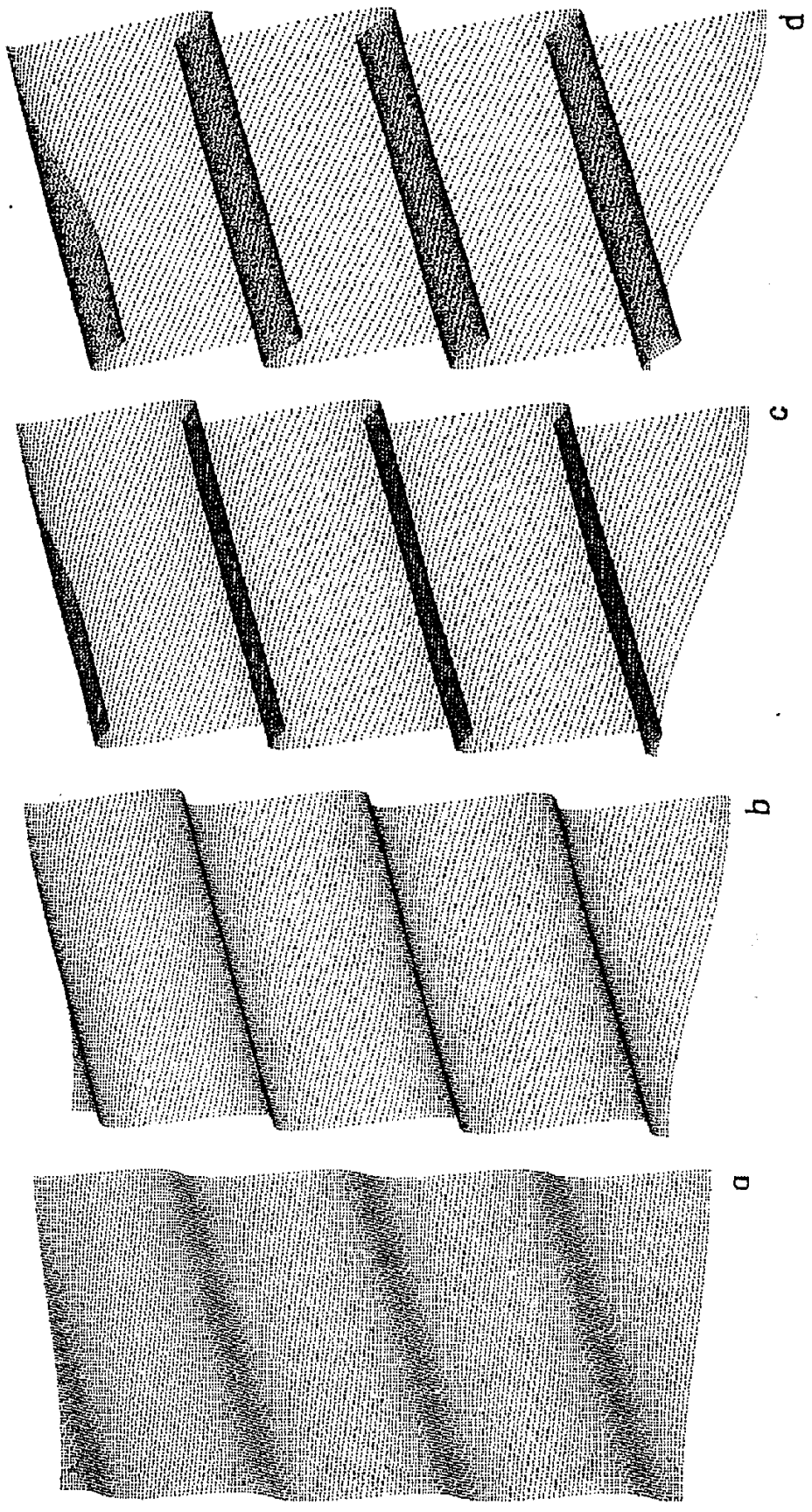

Fig. 7. Ray tracing maps with increasing film distance. a) 78, b) 156, c) 234, and d) 312 mm. Note the strong focussing in b). Other parameters are $a_t = 0.5$ nm, $\Lambda = 100$ µm, $\beta = 30°$, $\theta = 30°$

Obviously the longitudinal part of the Rayleigh wave can be omitted (which is no longer true with asymmetric reflections).

The "diffraction condition" $\boldsymbol{s}_h = \boldsymbol{s}_0 + \boldsymbol{h}$ for unit vectors $\boldsymbol{s}_0$ and $\boldsymbol{s}_h$ yields

$$h^2 = -2\boldsymbol{s}_0 \cdot \boldsymbol{h} ,$$

$$\boldsymbol{h} = -2(\boldsymbol{s}_0 \cdot \boldsymbol{n})\,\boldsymbol{n} ,$$

$$\boldsymbol{h} = \begin{pmatrix} 2a_t K \sin \Phi \sin\theta \cos\beta \\ 2a_t K \sin \Phi \sin\theta \sin\beta \\ 2\sin\theta - 2\cos\theta(\, a_t K \sin\Phi \cos\beta - \psi) \end{pmatrix}. \tag{9}$$

Then we can determine the direction $\boldsymbol{s}_h$ of the reflected ray

$$\boldsymbol{s}_h = \begin{pmatrix} \cos\theta - \psi \sin\theta + 2a_t K \sin\Phi \sin\theta \cos\beta \\ \varphi + 2a_t K \sin\Phi \sin\theta \sin\beta \\ \sin\theta + \psi\cos\theta + 2a_t K \sin\Phi \cos\theta \cos\beta \end{pmatrix}. \tag{10}$$

The film is located a distance D away from the origin and is perpendicular to $\hat{\mathbf{s}}_h = (\cos\theta, 0, \sin\theta)$ so that any point $\boldsymbol{r}_f$ on the film fulfils the relation $\boldsymbol{r}_f \cdot \hat{\mathbf{s}}_h = D$. The reflected ray with direction $\boldsymbol{s}_h$ coming from $\boldsymbol{r}_c$ hits the film at

$$\boldsymbol{r}_f = \boldsymbol{r}_c + t\boldsymbol{s}_h , \tag{11}$$

where $t = D + L\psi/\tan\theta$. The vector $\boldsymbol{r}_f - (D\cos\theta, 0, D\sin\theta)$ lies in the film plane and leads to the film coordinates by setting

$$x_f = r_{f,y} ,$$

$$y_f = \sqrt{(r_{f,x} - D\cos\theta)^2 + (r_{f,z} - D\sin\theta)^2} .$$

From (12) and (13) we finally have

$$\begin{aligned} x_f &= (L + D)\,\varphi + 2Da_t K \sin\Phi \sin\theta \sin\beta , \\ y_f &= (L + D)\,\psi - 2Da_t K \sin\Phi \cos\beta . \end{aligned} \tag{12}$$

Fig. 7 shows some ray tracing maps for different crystal to film distances. The troughs of the surface wave focus the reflected waves at a certain distance, whereas the crests defocus, resulting in a non-sinusoidal pattern with Λ-periodicity.

Lines of constant Φ which on the crystal surface form an angle β towards the y-axis are imaged on the film with an angle α towards the x_f-axis. These two angles are related by

$$\tan\alpha = \sin\theta \tan\beta . \tag{13}$$

In order to calculate the local intensity we have to determine the area on the film illuminated by an incident ray bundle confined to the solid angle $\mathrm{d}\psi\,\mathrm{d}\varphi$. This area $\mathrm{d}F$ is obtained by

$$\begin{aligned} \mathrm{d}F &= \left| \frac{\partial(x_f, y_f)}{\partial\psi} \times \frac{\partial(x_f, y_f)}{\partial\varphi} \right| \mathrm{d}\psi\,\mathrm{d}\varphi \\ &= \left| (L + D)^2 + 2D(L + D)\, a_t L K^2 \cos\Phi \left(\sin\theta \sin^2\beta + \frac{\cos^2\beta}{\sin\theta} \right) \right| \mathrm{d}\psi\,\mathrm{d}\varphi . \end{aligned} \tag{14}$$

With the area $dF_0 = (L + D)^2 \, d\psi \, d\varphi$ corresponding to zero amplitude we find the intensity ratio

$$\frac{I}{I_0} = \frac{dF_0}{dF} = \left[1 + 2Da_t K^2 \cos \Phi \left(\sin\theta \sin^2\beta + \frac{\cos^2\beta}{\sin\theta}\right) \frac{L}{L+D}\right]^{-1}. \tag{15}$$

An analytical expression of the dependence of I/I_0 on the film coordinates rather than on the incidence parameters cannot be given, as the reverse function of (15) is multivalued beyond a certain distance D_F, the focal distance. For $D > D_F$ several contributions to the intensity must be added in certain areas (see Fig. 7).

The focal distance is found by setting $\cos \Phi = -1$, $dF = 0$ and assuming $D \ll L$ which leads to

$$D_F = \sin\theta [2a_t K^2 (\sin^2\theta \sin^2\beta + \cos^2\beta)]^{-1}. \tag{16}$$

With $K = 2\pi/\Lambda$ we find for the extreme cases $\beta = 0°$ and $\beta = 90°$

$$D_F(\beta = 0°) = \frac{\Lambda^2 \sin\theta}{8\pi^2 a_t}, \tag{17}$$

$$D_F(\beta = 90°) = \frac{\Lambda^2}{8\pi^2 a_t \sin\theta}. \tag{18}$$

With $\theta = 37.5°$ and $\Lambda = 100$ μm a focal distance $D_F = 20$ cm is achieved by an amplitude as low as 0.38 nm ($\beta = 0$) or 1.04 nm ($\beta = 90°$), respectively.

For a given amplitude a wave travelling oblique to the scattering plane gives a weaker contrast than one with a parallel direction. This must be kept in mind when looking for scattered waves with different directions.

From (5) we may calculate the amplitude a_t for the 35 MHz IDT. With $\omega = 2\pi \cdot 35.4 \times 10^6 \, s^{-1}$, a measured impedance $G(\omega) = 0.43$ mS, and an IDT aperture $a = 1.57 \times 10^{-3}$ m we find $a_t/U_{in} = 0.092$ nm/V. Fig. 8. shows for a fixed distance D and varying voltage U_{in} the densitometer tracks of the SAW contrast observed under $\beta = 90°$. They are compared with theoretical curves obtained from (15). In addition an extended source was taken into account by convolution with the geometrical image of the source produced on the film by reflection through one point on the crystal surface. The agreement is quite satisfactory.

By finding the focal distance D_F and measuring the acoustic wavelength Λ as well as the angles θ and β, the acoustic amplitude a_t can be determined in a straigthforward manner. Unfortunately a source size of a few tenths of a millimeter is required for a precise determination of small amplitudes due to the increasing focal distance and the simultaneously increasing source image. A small pinhole close to the source is necessary in case of DORIS to perform these measurements with sufficient accuracy.

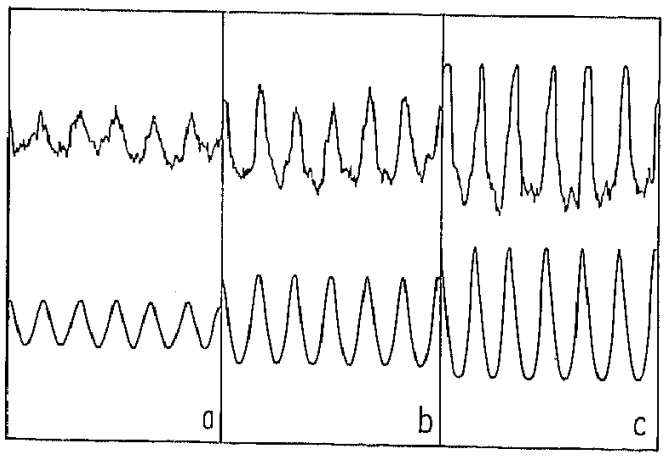

Fig. 8. Comparison of densitometer curves with theoretical curves. The input voltage has the following values: a) $U_{in} = 2.5$, b) 5.0, c) 7.5 V. The distance D was fixed at 18 cm, the Bragg angle $\theta = 45°$ and $\beta = 90°$. The intensity curves calculated for a point source are oonvoluted with a source width of 3 mm corresponding to an image width of 16 μm

Acknowledgements

We thank R. Veith and his coworkers of the Siemens AG, München, for the crystals, the possibility to use their facilities for preparation and fruitful discussions. One of us (H.C.) thanks DESY for financial support during his stay at Hamburg. This work was part of the project No. P. 4937 of the Austrian Fond zur Förderung der wissenschaftlichen Forschung.

References

[1] C.-C. Glüer, W. Graeff, and H. Möller, Proc. Internat. Conf. X-Ray and VUV Synchrotron Radiation Instrumentation, Hamburg 1982, in: Nuclear Instrum. and Methods 208, 701 (1983).
[2] R. W. Whatmore, P. A. Goddard, B. K. Tanner, and G. F. Clark, Nature 299, 44 (1982).
[3] R. W. Whatmore, P. A. Goddard, and B. K. Tanner, IEEE Ultrasonics Symp. Proc., San Diego, Vol. 1, 1982 (p. 363).
[4] H. P. Feuerbaum, G. Eberharter, and G. Tobolka, Scanning Electron Microscopy 1, 503 (1980).
[5] G. Eberharter and H. P. Feuerbaum, Appl. Phys. Letters 37, 698 (1980).
[6] A. A. Oliner (Ed.), Topics in Applied Physics, Vol. 24, Springer-Verlag, 1978.
[7] N. H. C. Reilly, R. F. Milsom, and M. Redwood, Electronics Letters 9, 419 (1973).
[8] U. Bonse and W. Graeff, Z. Naturf. 28a, 558 (1973).
[9] U. Bonse, Z. Phys. 177, 543 (1964).

(Received September 5, 1983)